

Solar Neutrino Detection Sensitivity in DARWIN via Electron Scattering

arXiv:2006.03114v1 [physics.ins-det] 4 Jun 2020

J. Aalbers¹, F. Agostini², S. E. M. Ahmed Maouloud³, M. Alfonsi⁴, L. Althueser⁵,
F. Amaro⁶, J. Angevaere⁷, V. C. Antochi¹, B. Antunovic^{8,†}, E. Aprile⁹, L. Arazi¹⁰,
F. Arneodo¹¹, M. Balzer¹², L. Baudis¹³, D. Baur¹⁴, M. L. Benabderrahmane¹¹,
Y. Biondi¹³, A. Bismark^{14,13}, C. Bourgeois¹⁵, A. Breskin¹⁰, P. A. Breur⁷, A. Brown¹³,
E. Brown¹⁶, G. Bruno¹¹, S. Brünner⁷, G. Bruno¹¹, R. Budnik¹⁰, C. Capelli¹³, J. Cardoso⁶,
D. Cichon¹⁷, M. Clark¹⁸, A. P. Colijn^{7,‡}, J. Conrad^{1,§}, J. J. Cuenca-García¹⁹,
J. P. Cussonneau²⁰, M. P. Decowski⁷, A. Depoian¹⁸, J. Dierle¹⁴, P. Di Gangi²,
A. Di Giovanni¹¹, S. Diglio²⁰, D. Douillet¹⁵, G. Drexlin²¹, K. Eitel¹⁹, R. Engel¹⁹,
E. Erdal¹⁰, A. D. Ferella^{22,23}, H. Fischer¹⁴, P. Fischer²⁴, W. Fulgione²⁵, P. Gaemers⁷,
M. Galloway¹³, F. Gao⁹, D. Giovagnoli²⁰, F. Girard¹³, R. Glade-Beucke¹⁴, F. Glück¹⁹,
L. Grandi²⁶, S. Grohmann²⁷, R. Gröbke¹⁹, R. Gumbsheimer¹⁹, V. Hannen⁵,
S. Hansmann-Menzemer²⁴, C. Hils⁴, B. Holzapfel²⁷, J. Howlett⁹, G. Iaquaniello¹⁵,
F. Jörg¹⁷, M. Keller²⁴, J. Kellerer²¹, G. Khundzakishvili¹⁸, B. Kilminster¹³, M. Kleifges¹²,
T. K. Kleiner²¹, G. Koltmann¹⁰, A. Kopec¹⁸, A. Kopmann¹², L. M. Krauss²⁸, F. Kuger¹⁴,
L. LaCascio²¹, H. Landsman¹⁰, R. F. Lang¹⁸, S. Lindemann¹⁴, M. Lindner¹⁷,
F. Lombardi⁶, J. A. M. Lopes^{6,¶}, A. Loya Villalpando⁷, Y. Ma²⁹, C. Macolino¹⁵,
J. Mahlstedt¹, A. Manfredini¹³, T. Marrodán Undagoitia¹⁷, J. Masbou²⁰, D. Masson¹⁴,
E. Masson¹⁵, N. McFadden¹³, P. Meinhardt¹⁴, R. Meyer⁴, B. Milosevic⁸, S. Milutinovic⁸,
A. Molinario²⁵, C. M. B. Monteiro⁶, K. Morá⁹, E. Morteau²⁰, Y. Mosbacher¹⁰,
M. Murra⁵, J. L. Newstead³⁰, K. Ni²⁹, U. G. Oberlack⁴, M. Obradovic⁸, K. Odgers¹⁶,
I. Ostrovskiy³¹, J. Palacio²⁰, M. Pandurovic⁸, B. Pelsers¹, R. Peres¹³, J. Pienaar²⁶,
M. Pierre²⁰, V. Pizzella¹⁷, G. Plante⁹, J. Qi²⁹, J. Qin¹⁸, D. Ramírez García¹⁴,
S. E. Reichard^{a,13}, N. Rupp¹⁷, P. Sanchez-Lucas¹³, J. Santos⁶, G. Sartorelli², D. Schulte⁵,
H.-C. Schultz-Coulon²⁴, H. Schulze Eißing⁵, M. Schumann¹⁴, L. Scotto Lavina³,
M. Selvi², P. Shagin³², S. Sharma²⁴, W. Shen²⁴, M. Silva⁶, H. Simgen¹⁷, M. Steidl¹⁹,
S. Stern²¹, D. Subotic⁸, P. Szabo¹⁰, A. Terliuk²⁴, C. Therreau²⁰, D. Thers²⁰, K. Thieme¹³,
F. Toennies¹⁴, R. Trotta^{33,||}, C. D. Tunnell³², K. Valerius¹⁹, G. Volta¹³, D. Vorkapic⁸,
M. Weber¹², Y. Wei²⁹, C. Weinheimer⁵, M. Weiss¹⁰, D. Wenz¹⁴, C. Wittweg⁵, J. Wolf²¹,
S. Wuestling¹², M. Wurm⁴, Y. Xing²⁰, T. Zhu⁹, Y. Zhu²⁰, J. P. Zopounidis³, K. Zuber³⁴
(DARWIN Collaboration^b)

¹Oskar Klein Centre, Department of Physics, Stockholm University, AlbaNova, Stockholm SE-10691, Sweden

²Department of Physics and Astronomy, University of Bologna and INFN-Bologna, 40126 Bologna, Italy

³LPNHE, Université Pierre et Marie Curie, Université Paris Diderot, CNRS/IN2P3, Paris 75252, France

⁴Institut für Physik & Exzellenzcluster PRISMA⁺, Johannes Gutenberg-Universität Mainz, 55099 Mainz, Germany

⁵Institut für Kernphysik, Westfälische Wilhelms-Universität Münster, 48149 Münster, Germany

⁶LIBPhys, Department of Physics, University of Coimbra, 3004-516 Coimbra, Portugal

⁷Nikhef and the University of Amsterdam, Science Park, 1098XG Amsterdam, Netherlands

⁸Vinca Institute of Nuclear Science, University of Belgrade, Mihajla Petrovica Alasa 12-14. Belgrade, Serbia

- ⁹Physics Department, Columbia University, New York, NY 10027, USA
¹⁰Department of Particle Physics and Astrophysics, Weizmann Institute of Science, Rehovot 7610001, Israel
¹¹New York University Abu Dhabi, Abu Dhabi, United Arab Emirates
¹²Institute for Data Processing and Electronics (IPE), Karlsruhe Institute of Technology (KIT), 76344 Eggenstein-Leopoldshafen, Germany
¹³Physik-Institut, University of Zurich, 8057 Zurich, Switzerland
¹⁴Physikalisches Institut, Universität Freiburg, 79104 Freiburg, Germany
¹⁵Université Paris-Saclay, CNRS/IN2P3, IJCLab, F-91405 Orsay, France
¹⁶Department of Physics, Applied Physics and Astronomy, Rensselaer Polytechnic Institute, Troy, NY 12180, USA
¹⁷Max-Planck-Institut für Kernphysik, 69117 Heidelberg, Germany
¹⁸Department of Physics and Astronomy, Purdue University, West Lafayette, IN 47907, USA
¹⁹Institute for Nuclear Physics (IKP), Karlsruhe Institute of Technology (KIT), 76344 Eggenstein-Leopoldshafen, Germany
²⁰SUBATECH, IMT Atlantique, CNRS/IN2P3, Université de Nantes, Nantes 44307, France
²¹Institute of Experimental Particle Physics (ETP), Karlsruhe Institute of Technology (KIT), 76344 Eggenstein-Leopoldshafen, Germany
²²Department of Physics and Chemistry, University of L'Aquila, 67100 L'Aquila, Italy
²³INFN-Laboratori Nazionali del Gran Sasso and Gran Sasso Science Institute, 67100 L'Aquila, Italy
²⁴Physikalisches Institut, Ruprecht-Karls-Universität Heidelberg, Heidelberg, Germany
²⁵INFN-Laboratori Nazionali del Gran Sasso and Gran Sasso Science Institute, 67100 L'Aquila, Italy
²⁶Department of Physics & Kavli Institute for Cosmological Physics, University of Chicago, Chicago, IL 60637, USA
²⁷Institute for Technical Physics (ITEP), Karlsruhe Institute of Technology (KIT), 76344 Eggenstein-Leopoldshafen, Germany
²⁸The Origins Project Foundation, Phoenix, AZ 85020, USA
²⁹Department of Physics, University of California, San Diego, CA 92093, USA
³⁰School of Physics, The University of Melbourne, Victoria 3010 Australia
³¹Department of Physics, University of Alabama, Tuscaloosa, AL 35487, USA
³²Department of Physics and Astronomy, Rice University, Houston, TX 77005, USA
³³Department of Physics, Imperial Centre for Inference and Cosmology, Imperial College London, London SW7 2AZ, UK
³⁴Institute for Nuclear and Particle Physics, TU Dresden, 01069 Dresden, Germany

Received: date / Accepted: date

Abstract We detail the sensitivity of the liquid xenon (LXe) DARWIN observatory to solar neutrinos via elastic electron scattering. We find that DARWIN will have the potential to measure the fluxes of five solar neutrino components: pp , ${}^7\text{Be}$, ${}^{13}\text{N}$, ${}^{15}\text{O}$ and pep . The precision of the ${}^{13}\text{N}$, ${}^{15}\text{O}$ and pep components is hindered by the double-beta decay of ${}^{136}\text{Xe}$ and, thus, would benefit from a depleted target. A high-statistics observation of pp neutrinos would allow us to infer the values of the weak mixing angle, $\sin^2 \theta_w$, and the electron-type neutrino survival probability, P_e , in the electron recoil energy region from a few keV up to 200 keV for the first time, with relative precision of 5% and 4%, respectively, at an exposure of 300 ty. An observation of pp and ${}^7\text{Be}$ neutrinos would constrain the neutrino-inferred solar luminosity down to 0.2%. A combination of all flux measurements would distinguish between the high (GS98) and low metallicity (AGS09) solar models with 2.1-2.5 σ significance, independent of external measurements from other experi-

ments or a measurement of ${}^8\text{B}$ neutrinos through coherent elastic neutrino-nucleus scattering in DARWIN. Finally, we demonstrate that with a depleted target DARWIN may be sensitive to the neutrino capture process of ${}^{131}\text{Xe}$.

Keywords Neutrino, Sun, Dark Matter, Direct Detection, Xenon

1 Introduction

Current and future LXe direct detection dark matter experiments, such as XENONnT, LZ [1], and DARWIN [2], will exhibit sensitivity to neutrinos at the $\sim\text{MeV}$ scale. Typically, neutrinos have been regarded as backgrounds in the search for dark matter (DM) [3, 4]; but, as signals, they present opportunities to characterize their sources and pursue physics beyond the Standard Model (SM) [5–10]. While DM remains the primary objective, detectors with multi-tonne (t) xenon targets will seek neutrino signals without the need for additional investments.

Solar neutrinos, in particular, are observable in dark matter detectors through two types of interactions: elastic electron scattering (ES) and coherent elastic neutrino-nucleus scattering (CEvNS) [11, 12]. In the SM, ES occurs with the exchange of a Z or W boson. The latter is only possible for ν_e , which creates nearly an order of magnitude of difference

^ashayne@physik.uzh.ch

^bdarwin@lngs.infn.it

[†]Also at University of Banja Luka, Bosnia and Herzegovina

[‡]Also at Institute for Subatomic Physics, Utrecht University, Utrecht, Netherlands

[§]Wallenberg Academy Fellow

[¶]Also at Coimbra Polytechnic - ISEC, Coimbra, Portugal

^{||}Also at SISSA, Data Science Excellence Department, Trieste, Italy

between the interaction rates of ν_e and $\nu_{\mu,\tau}$. On the other hand, CEvNS occurs only through the exchange of a Z boson, with an interaction cross section that is strongly determined by the target's neutron number. With their different sensitivity to the solar neutrino flux, these two channels provide complementarity over a wide range of energies.

Dedicated solar neutrino experiments have made numerous observations of ES with water, heavy water, and liquid scintillator targets. Borexino independently measured the fluxes of the lower-energy pp [13], ${}^7\text{Be}$ [14], and pep [15] components. Subsequently, Borexino presented the first results from simultaneous spectroscopy of these three components above 0.19 MeV, yielding the most precise measurements to date as well as an upper limit on the combined carbon, nitrogen and oxygen (CNO) flux that is ~ 4 times higher than predicted in the Standard Solar Model (SSM) [16, 17]. Five experiments, Borexino [18, 19], Super-K [20], KamLAND [21], SNO [22], and SNO+ [23], have measured the higher-energy ${}^8\text{B}$ flux. COHERENT made the first observation of CEvNS [24], but astrophysical neutrinos have yet to be detected in this way.

After decades of investigation, important questions about our Sun persist. From an astrophysical perspective, the most salient issue lies in the solar abundance problem. The more recent low-metallicity (low-Z) AGSS09 SSM [25, 26] would seem to better represent the photosphere than its predecessor, the high-metallicity (high-Z) GS98 SSM [25, 27]. However, a comparison of individual flux measurements with theoretical predictions tends to favor the high-Z SSM, contradicting the common assumption that abundances in the radiative envelope are the same as those in the photosphere. This preference is further supported by helioseismic data that have long since disfavored a low-Z model [28]. As carbon, nitrogen and oxygen constitute the majority of heavy elements in the Sun, their neutrino fluxes are the most sensitive to metallicity. A combined analysis of available measurements remains inconclusive, but a relative uncertainty of $\sim 15\%$ on a combined CNO flux measurement would begin to favor one model over the other [17, 29, 30]. While less sensitive to metallicity than CNO neutrinos, an improved measurement of the ${}^8\text{B}$ flux would also help to distinguish them.

Measurements of electroweak parameters play an important role in our understanding of the SM and our search for new physics [31, 32]. Non-standard neutrino interactions (NSI) might modify the Large Mixing Angle (MSW-LMA) solution to the solar neutrino problem. Solar neutrinos serve as one probe to observe or set bounds on NSI. Two of these parameters, the weak mixing angle ($\sin^2 \theta_w$) and the ν_e survival probability (P_e), may be measured with the ES process. On one hand, atomic parity violation in cesium at 2.4 MeV yields the lowest energy at which $\sin^2 \theta_w$ has been measured [33]. On the other, Borexino has provided the lowest-energy measurement of the ν_e survival probability extracted from the

tail of the proton-proton distribution (>0.19 MeV) [17]. No experiment, thus far, has been able to access energies below these respective thresholds. DARWIN will measure $\sin^2 \theta_w$ and P_e for the first time in the energy region [1,200] keV.

In this manuscript, we highlight the efficacy with which DARWIN will shed light on solar and neutrino physics through elastic electron scattering. We first detail its sensitivity to each component of the solar neutrino flux. Then, we illustrate the precision with which DARWIN could reconstruct $\sin^2 \theta_w$ and P_e in the low energy range [1,200] keV. Lastly, we demonstrate how a combined analysis of neutrino flux measurements would resolve the solar abundance problem.

2 The DARWIN Experiment

The DARWIN observatory is a next-generation dark matter experiment that will operate with 50 t (40 t active) of xenon in a cylindrical, dual-phase time projection chamber (TPC) that is 2.6 m in both height and diameter [2]. The TPC will be placed underground in a double-walled cryostat vessel shielded by water Cherenkov and neutron vetoes that enable us to observe cosmogenic muons and their progeny. The TPC will be equipped to read out both light and charge signals.

A charged particle that interacts in liquid xenon (LXe) produces photons (scintillation) and electrons (ionization). The TPC promptly detects these photons as an ‘‘S1’’ scintillation signal with photosensors instrumented in arrays at the top and bottom of the target region. An applied electric field drifts the electrons upward and extracts them into the gas phase, where electroluminescence generates an amplified ‘‘S2’’ scintillation signal. The radial position of an interaction is reconstructed with the S2 light pattern in the top array, while its depth is inferred from the time delay between S1 and S2. Together, S1 and S2 reconstruct the energy of the event with excellent resolution. The ratio S2/S1 discriminates between scatters off electrons and those off nuclei. The combination of position, energy and discrimination allows for strong event selections to mitigate sources of background.

The most troublesome background for a solar neutrino search (ES) arises from the ${}^{222}\text{Rn}$ emanated by detector components. More precisely, the ${}^{214}\text{Pb}$ daughter decays directly to ${}^{214}\text{Bi}$ with a branching ratio of 11%, emitting a lone β with an energy up to $Q = 1.02$ MeV [34]. Otherwise, ${}^{214}\text{Pb}$ decays to an excited state of ${}^{214}\text{Bi}$ that emits a γ coincident with the β to create a sharp rise above the lone- β continuum. There are several excited states that contribute, starting at 0.274 MeV, as illustrated in Figure 1. With a long half-life (3.8 d), ${}^{222}\text{Rn}$ distributes itself homogeneously in the LXe volume, such that it is not reduced with the deliberate selection of an inner volume, known as fiducialization. The detector materials in DARWIN will be carefully selected for low radon emanation through a dedicated radioassay program, as

in XENON1T/nT [35]. DARWIN will deploy a radon distillation column to further reduce the radon level. Cryogenic distillation was successfully applied in XENON100 [36] and XENON1T [37] to reduce radon levels. For DARWIN, we assume a target ^{222}Rn activity of $0.1 \mu\text{Bq/kg}$.

A second background comes from intrinsic ^{85}Kr , a β emitter ($Q = 0.687 \text{ MeV}$; $T_{1/2} = 10.8 \text{ y}$) that remains in the xenon volume after extraction from the atmosphere. As with ^{222}Rn , ^{85}Kr homogeneously distributes itself in the LXe volume. XENON1T has already demonstrated a concentration $\text{natKr/Xe} < 360 \text{ ppq}$ [38]. Krypton may be further reduced at any time via online distillation, as applied in XENON1T [37]. We assume a concentration of 2 ppq in this study, but find that it has a negligible effect even at its current level.

Long-lived radionuclides in detector materials constitute a third class of background events. The decay chains of ^{238}U , ^{232}Th and ^{235}U generate various α and β particles as well as γ rays. The main contributors of γ rays from these three chains are ^{214}Bi (2.45 MeV) and ^{208}Tl (2.61 MeV), including the background induced by decays in the non-instrumented xenon volume around the TPC. Additional γ rays are emitted in the decays of ^{137}Cs (0.662 MeV), ^{40}K (1.46 MeV), and the daughters of ^{60}Co (1.17 and 1.33 MeV) and ^{44}Ti (2.66 MeV). The α and β particles do not travel far and thus are eliminated with fiducialization. The γ rays, however, penetrate the innermost region, where they experience photoabsorption or Compton scattering. The more notable contributors have historically been the stainless steel cryostat and photosensors [35]. We include a materials background component derived from the DARWIN simulation in [39], which considers a more radiopure titanium cryostat. The simulation is adapted to this case by incorporating position-dependent multiscatter resolution, 3-15 mm, and selecting events within a 30 t super-ellipsoidal fiducial volume that minimizes the contribution of these Compton scatters below 200 keV. With 10 live years of data, we would accrue 300 tonne-years (ty) of exposure, compared to the 200 ty goal for the dark matter search.

Finally, unstable xenon isotopes pose a potential background in the search for ES of solar neutrinos. The isotope ^{136}Xe , which occurs naturally with an abundance of 8.9%, undergoes double-beta decay ($Q = 2.46 \text{ MeV}$; $T_{1/2} = 2.17 \cdot 10^{21} \text{ y}$). The resultant spectrum circumscribes the entire signal region of interest. Furthermore, the muon-induced neutron capture process of ^{136}Xe creates ^{137}Xe , which then beta decays ($Q = 4.16 \text{ MeV}$; $T_{1/2} = 3.82 \text{ min}$). The impact of ^{137}Xe proves to be negligible at the level of 10^{-3} per tonne-year per keV, three orders of magnitude lower than ^{136}Xe double-beta decay [39]. These ^{136}Xe background contributions are removable through isotopic depletion; however, depletion would diminish the prospects for a neutrinoless double-beta search with ^{136}Xe in DARWIN [39]. Lastly, ^{124}Xe decays via double electron capture ($T_{1/2} =$

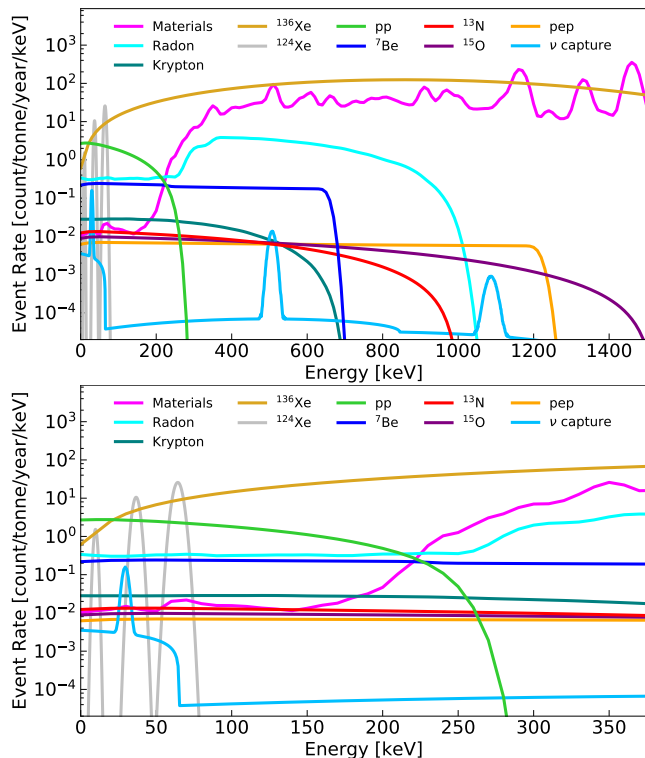


Fig. 1 (top) The electron recoil spectra of five solar neutrino components, neutrino capture on ^{131}Xe (solid), and five backgrounds (dashed) up to 1.5 MeV. The solar components follow from the high-Z SSM model. The materials and ^{136}Xe events in [1.5,3] MeV (not shown) are also used in the statistical analysis. The materials component includes events in a 30 t fiducial volume. (bottom) A zoomed spectrum of the lower energy components.

$1.4 \cdot 10^{22} \text{ y}$) [40, 41], as first observed in XENON1T [42]. The subsequent cascade of Auger electrons and X-rays is observed as a single peak at 64.3 (36.7; 9.8) keV with a branching ratio of 0.75 (0.23; 0.017), following the fast atomic process and their sub-millimeter spread in liquid xenon. With an abundance of 0.1%, one expects a total of 228 double electron capture events per tonne-year.

3 Solar Neutrinos in DARWIN

DARWIN will be optimized for the detection of low-energy nuclear recoils. This fact also implies that DARWIN will be well equipped to detect ES with high efficiency and excellent energy resolution. In the following, we calculate the expected event rates for the individual solar components.

The spectral fluxes of pp , ^{13}N , and ^{15}O neutrinos are represented with the β form,

$$\frac{d\Phi_i}{dE_\nu} = \Phi_i A (x_i - E_\nu) [(x_i - E_\nu)^2 - m_e^2]^{\frac{1}{2}} E_\nu^2, \quad (1)$$

where $x_i \equiv Q_i + m_e$, Q_i and Φ_i are the characteristic maximal energy and the flux scale of neutrino component i , respec-

component	$\Phi[\text{cm}^{-2}\text{s}^{-1}]$	σ [%]	$Q[\text{keV}]$	P_e
pp	$5.98 \cdot 10^{10}$	0.6	420	0.55
^7Be	$4.93 \cdot 10^9$	6	862, 384	0.52
^{13}N	$2.78 \cdot 10^8$	15	1200	0.52
^{15}O	$2.05 \cdot 10^8$	18	1732	0.50
pep	$1.44 \cdot 10^8$	1	1442	0.50

Table 1 The characteristic values of the flux scales [43], maximum neutrino energies and MSW-LMA ν_e survival probability [44] used in this study.

tively, m_e is the electron mass, A is the corresponding normalization factor, and E_ν is the energy of the emitted neutrino. In contrast, ^7Be and pep neutrinos are monoenergetic. The ^7Be neutrinos are emitted at 0.862 MeV (0.384 MeV) with a branching ratio of 90% (10%), while the pep neutrinos have an energy of 1.44 MeV. The flux scales are taken from the high-metallicity solar model [43].

These spectral fluxes are convolved with the differential cross section of elastic electron-neutrino scattering:

$$\frac{dR_i}{dE_r} = N_e \sum_j \int P_{ej} \frac{d\Phi_i}{dE_\nu} \frac{d\sigma_j}{dE_r} dE_\nu, \quad (2)$$

where P_{ej} is the oscillation probability of lepton flavor j to the electron neutrino, N_e is the number of target electrons per tonne of xenon, and E_r is the energy of the induced recoil. The flux scales, maximum neutrino energies and survival probabilities are listed in Table 1. The survival probabilities follow the MSW-LMA solution at low energies in the vacuum-dominated regime [44]. The differential cross section is given by [45, 46]

$$\frac{d\sigma}{dE_r} = \frac{2G_F^2 m_e}{\pi} \left[g_L^2 + g_R^2 \left(1 - \frac{E_r}{E_\nu} \right)^2 - g_L g_R \frac{m_e E_r}{E_\nu^2} \right], \quad (3)$$

with the coupling parameters $g_L = \sin^2 \theta_w - \frac{1}{2}$ and $g_R = \sin^2 \theta_w$. For the ν_e , $g_L \rightarrow g_L + 1$ to account for its charged current interactions. We assume $\sin^2 \theta_w = 0.2387$ [47]. We incorporate a step approximation according to the binding energies of electrons in the shells of a xenon atom, which leads to a small suppression of event rates below 35 keV. We also apply the Gaussian energy resolution obtained in XENON1T [48],

$$\frac{\sigma(E_r)}{E_r} = \frac{0.3171}{\sqrt{E_r[\text{keV}]} + 0.0015}. \quad (4)$$

The pp neutrinos constitute the most prominent component due to the low energy threshold achievable in LXe TPCs. Here, we assume a threshold at 1 keV, which yields an integrated rate of 365 events per tonne-year. This high rate presents an opportunity to probe $\sin^2 \theta_w$ for the first time below ~ 200 keV, to improve upon the precision of existing measurements of P_e at low energies, and to further constrain the neutrino-inferred measurement of solar luminosity.

The ^7Be neutrinos comprise the second most prominent component. The larger branch contributes 133 events per tonne-year, while the smaller one contributes 7.6 events. The ^7Be flux is more sensitive to solar metallicity and, as such, it may be combined with a high-precision measurement of the pp flux to make an initial assessment of different metallicity models.

The third most prominent components are those of ^{13}N , ^{15}O , and pep , which induce 6.5, 7.1 and 7.6 events per tonne-year, respectively. Despite having the lowest rate, ^{13}N events fall within a narrower energy range than either ^{15}O or pep , such that the ^{13}N spectrum rises above both below ~ 0.4 MeV. Consequently, it is possible for DARWIN to make the first statistically significant observation of CNO neutrinos by exploiting higher statistics at lower energies. As the most sensitive to metallicity, being 30% higher in the high-Z scenario, measurements of the ^{13}N and ^{15}O fluxes would greatly enhance the capability to distinguish between solar models. The rates of ^{17}F , ^8B and hep neutrinos are negligible.

Finally, we consider neutrino capture on ^{131}Xe ($Q = 0.355$ MeV), the only isotope with a sufficiently low Q -value to exhibit sensitivity to solar neutrinos. The expected observable signature consists of two signals: a prompt electron and a combination of X-rays and Auger electrons that are emitted together in the subsequent electron capture (EC) decay of $^{131}\text{Cs}^+$ ($T_{1/2} = 9.69$ days). The prompt electrons would create a spectrum that mirrors those of the spectral neutrino fluxes shifted to lower energies by the Q -value of this reaction ($E_e = E_\nu - Q$). The EC decay would appear as a Gaussian peak at 0.030 MeV. The long half-life of the EC process precludes delayed coincidence of these two signatures. The contribution of each solar component (including ^8B) follows from [49]. There are three distinct peaks visible in Figure 1. The two higher energy peaks come from capturing the monoenergetic ^7Be and pep neutrinos; while the peak below 50 keV is the combination of EC, the lower branch of ^7Be , and the tail of the pp spectrum. With a ^{131}Xe abundance of 21.2%, we expect 1.23 neutrino capture events per tonne-year.

4 Flux and Luminosity

Having defined the signal and background models, we assess DARWIN's sensitivity to each of the neutrino components. We employ a full spectral fit of all components up to 3 MeV. A set of maximum likelihood estimators is determined for the 5-dimensional set of flux scale parameters, $\mathbf{f} = \{f_{pp}, f_{Be}, f_N, f_O, f_{pep}\}$, and the neutrino capture rate, f_{cap} , given the neutrino mixing parameters, $\theta = \{\sin^2 \theta_w, P_e\}$:

$$P(n_j | \mu_j(\mathbf{f}, f_{\text{cap}})) = \mathcal{L}(\mathbf{f}, f_{\text{cap}}) = \prod_{j=1}^n \frac{\mu_j^{n_j}}{n_j!} e^{-\mu_j}. \quad (5)$$

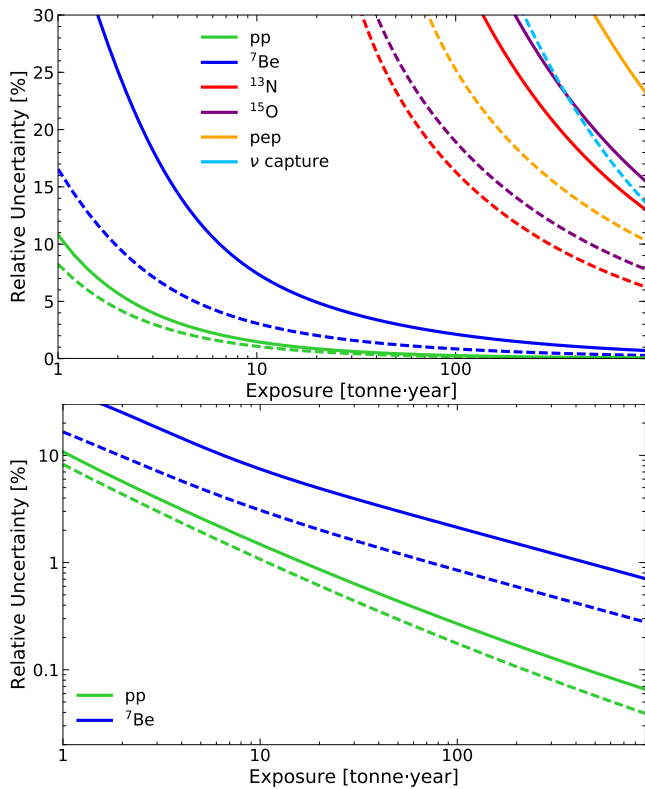


Fig. 2 The measured relative uncertainty of each solar neutrino component and neutrino capture as a function of exposure. The median fluxes of the high-Z model are assumed. Solid (dashed) curves correspond to a natural (depleted) target. A log scale of the pp and ^7Be components is shown in the bottom panel for clarity.

These parameters predict the average number of events in the j th energy bin, μ_j , while the observed number of events in that bin, n_j , is randomly sampled. The background-only region (>1.5 MeV) is used to constrain the uncertainties in the normalization of the materials and ^{136}Xe backgrounds at lower energies. All components are left free in the fitting routine.

We run toy experiments for each exposure in our range of interest, [1, 1000] (ty), to ascertain the expected relative 1σ uncertainties, σ_i , for each neutrino component. These values are shown in Figure 2 normalized to their respective median high-Z values. The solid lines correspond to a natural target, while the dashed lines indicate a target depleted of ^{136}Xe by two orders of magnitude.

With 1 ty, DARWIN would quickly match the precision of the pp flux (10%) currently set by Borexino. A subpercent measurement would follow with 20 ty, ultimately reaching 0.15% at 300 ty. Similarly, DARWIN would match Borexino's ^7Be measurement (2.7%) within 60 ty and then achieve 1% precision with 300 ty. The ^{13}N and ^{15}O neutrinos would also be attainable. The former (latter) would require 100 ty (200 ty) to reach 3σ detection with a natural xenon target. Finally, DARWIN could observe the pep component and

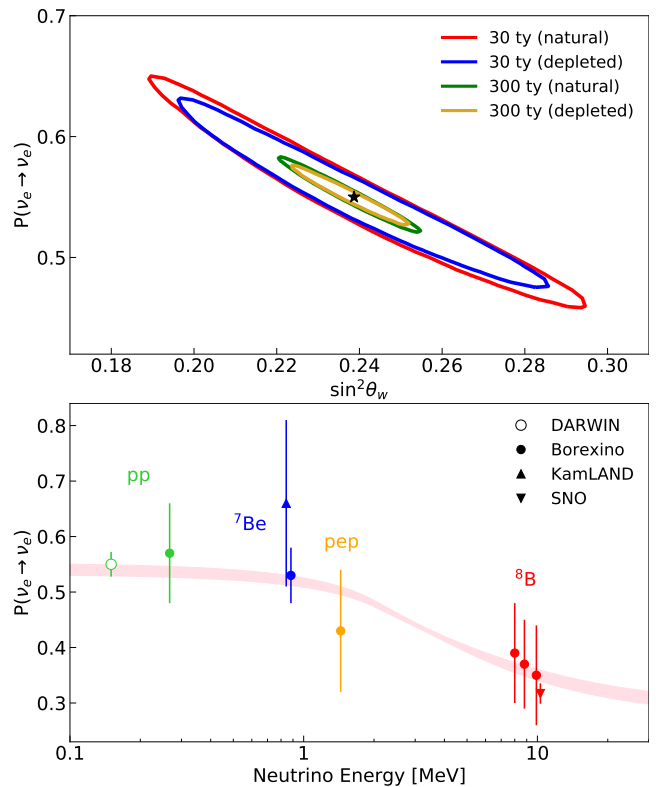


Fig. 3 (top) The 68% confidence regions of $\sin^2 \theta_w$ and P_e for two exposures and the two target compositions. (bottom) The ν_e survival probability versus neutrino energy under the high-Z SSM. Dots represent the solar measurements of pp (green), ^7Be (blue), pep (orange), and ^8B (red) from Borexino [17, 19]. The upward (downward) triangle shows a measurement of ^7Be (^8B) from KamLAND (SNO) [21, 22]. The open point indicates that DARWIN could enhance the precision of the ν_e survival probability to 0.02 below 200 keV using pp events. The pink band represents the 1σ prediction of the MSW-LMA solution [44].

neutrino capture with 60 ty and 200 ty, respectively, using a necessarily depleted target.

The solar luminosity inferred from solar neutrino data, $L_{\odot, \nu} / L_{\odot} = 1.04^{+0.07}_{-0.08}$, agrees with the measured (photon-inferred) solar luminosity within 7% [29]. The pp reaction contributes most strongly to the total energy generation in the Sun. Thus, high-precision measurements of the pp and ^7Be components, which respectively comprise 92% and 7.4% of the solar luminosity, would reduce this uncertainty. With the precision levels shown here, DARWIN would achieve an uncertainty of 0.2% on the neutrino-inferred solar luminosity.

5 Electroweak Parameters

Following a precise measurement of the pp component, we may infer the values of the weak mixing angle and the ν_e survival probability, as they directly affect the shape of its observed recoil spectrum. We adopt a likelihood function in which the two electroweak parameters are free to vary:

$$P(n_j | \mu_j(\theta)) = \mathcal{L}(\theta). \quad (6)$$

The presence of ${}^7\text{Be}$ neutrinos only slightly worsens the sensitivity to these parameters, while the other neutrino components have a negligible effect. The uncertainty in the pp flux contributes negligibly to the total uncertainty of $\sin^2\theta_w$ and P_e .

We find the maximum likelihood estimators of $\sin^2\theta_w$ and P_e in a series of toy experiments. From the resultant 2D distribution, we determine the 68% confidence regions as shown in Figure 3 (top) for four scenarios based on two exposures (30 and 300 ty) and two target compositions.

In the case of a natural target, DARWIN would reconstruct $\sin^2\theta_w$ and P_e with uncertainties as small as 0.0122 (5.1%) and 0.022 (4.0%), respectively. Alternatively, with a depleted target, the uncertainties would shrink to 0.0099 (4.2%) and 0.017 (3.1%). A measurement of $\sin^2\theta_w$ would be the first in this energy range, albeit with an uncertainty roughly five times higher than those at higher energies. A measurement of P_e would improve upon the existing one from Borexino by an order of magnitude. This projection is shown in Figure 3 (bottom) with solar neutrino measurements from Borexino [17, 19], KamLAND [21], and SNO [22].

6 Solar Abundance Problem

DARWIN may utilize a combination of neutrino flux measurements to probe the metallicity of the Sun. We repeat the sensitivity assessment of the flux measurements, \mathbf{f} described previously. In this instance, however, we allow the flux values derived from the high- and low-Z models to vary from their median values according to their respective theoretical uncertainties. We put these uncertainties, σ_i , into a multivariate (Gaussian) simulation characterized by a 5-dimensional matrix $\Sigma = [\rho_{ij}\sigma_i\sigma_j]$ that accounts for all correlations of the flux components, ρ_{ij} . The correlation values are based on [43]. For each trial at a given exposure, we use the randomly sampled \mathbf{f} to calculate its (squared) Mahalanobis distance $\delta^2 = (\mathbf{f} - 1)^T \cdot \Sigma^{-1} \cdot (\mathbf{f} - 1)$ [50], which quantifies the deviation from the true values. The simulation is repeated for both the high- and low-Z models. A p-value is calculated for each iteration of the high-Z simulation by integrating the low-Z distribution above the high-Z Mahalanobis value. We then take the median p-value from the final distribution.

Figure 4 displays the significance corresponding to these p-values as a function of exposure for the first pair of measurements, pp and ${}^7\text{Be}$, and for each subsequent addition of the other components. The ${}^{13}\text{N}$ component only modestly increases the exclusion potential due to the large uncertainties in both theory and experiment. The combination of both ${}^{13}\text{N}$ and ${}^{15}\text{O}$, however, yields a significant gain above ~ 10 ty. The pep component enhances the exclusion to 2.1σ (2.5σ) with a natural (depleted) target at an exposure of 300 ty.

DARWIN would remain limited by the ${}^{136}\text{Xe}$ background with a natural target, but with depletion it would distinguish

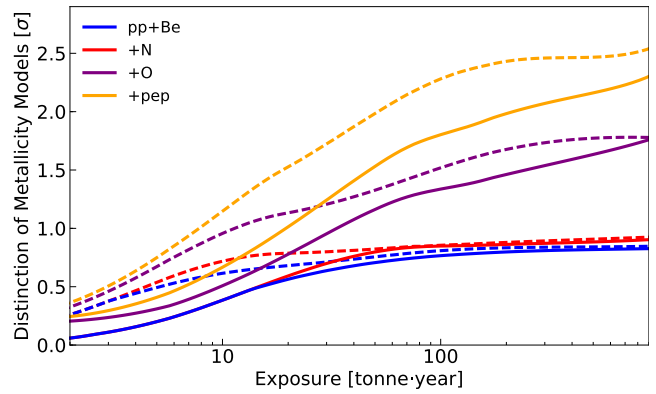


Fig. 4 The median significance with which the the high- and low-Z models may be distinguished is calculated for the first pair of flux measurements, pp and ${}^7\text{Be}$, as a function of exposure. Additional cases add ${}^{13}\text{N}$, ${}^{15}\text{O}$ and pep sequentially. The solid (dashed) curves correspond to a natural (depleted) xenon target.

between the high- and low-Z SSMs up to the theoretical uncertainties. The significance illustrated in Figure 4 may be further improved either with a measurement of the solar ${}^8\text{B}$ flux via CEvNS in DARWIN or with independent measurements from other experiments.

7 Outlook

The DARWIN observatory will feature sensitivity to five components of the solar flux via ES. A low energy threshold of 1 keV allows DARWIN to observe the majority of pp neutrinos, which have (mostly) eluded contemporary neutrino observatories. With 300 ty, we would be able to achieve 0.15% precision in the pp flux measurement, approximately two orders of magnitude better than the current precision from Borexino. DARWIN would improve upon existing measurements of the ${}^7\text{Be}$ flux by a factor of 3. These measurements, in turn, would reduce the uncertainty on the neutrino-inferred solar luminosity to 0.2%. The pep neutrinos may be observed with 3σ significance within the lifetime of the experiment, depending on the target composition. And, with only three years of data, DARWIN would make an observation of CNO neutrinos with 3σ significance.

Precise measurements of these solar components further extend the physics reach of DARWIN. The high-statistics pp events would provide the means to measure both $\sin^2\theta_w$ and P_e in an energy region that is yet to be probed. The better precision of P_e , in particular, would be up to one order of magnitude better than the current lowest-energy measurement from Borexino. All obtained measurements and limits on the fluxes would together provide information to distinguish between the high- and low-Z SSMs. These capabilities are dependent on the target composition. Only with a target depleted of ${}^{136}\text{Xe}$ by approximately two orders of magnitude would DARWIN make such precise measurements via ES or

exploit them to distinguish between solar models. DARWIN may further enhance its distinction power with a measurement of the ^8B flux via CEvNS. The forecast for such a measurement is highly sensitive to the achieved energy threshold for nuclear recoils, and it is left for a future study. A powerful physics case exists for the pursuit of solar neutrinos in DARWIN, and it comes without the need for additional investment beyond the option of depletion.

Acknowledgements

This work was supported by the Swiss National Science Foundation under grants No 200020-162501, and No 200020-175863, by the European Union's Horizon 2020 research and innovation programme under the Marie Skłodowska-Curie grant agreements No 674896, No 690575, and No 691164, by the European Research Council (ERC) grant agreements No 742789 (Xenoscope), and No 724320 (ULTIMATE), by the Max-Planck-Gesellschaft, by the Deutsche Forschungsgemeinschaft (DFG) under GRK-2149, by the US National Science Foundation (NSF) grants No 1719271, and No 1940209, by the Portuguese FCT, by the Netherlands Organisation for Scientific Research (NWO), by the Ministry of Education, Science and Technological Development of the Republic of Serbia and by grant ST/N000838/1 from Science and Technology Facilities Council (UK).

References

1. D. S. Akerib *et al.* (LUX-ZEPLIN Collaboration), [arXiv:1802.06039](#).
2. J. Aalbers *et al.* (DARWIN Collaboration), *JCAP* **1611**, 017 (2016), [arXiv:1606.07001](#).
3. L. E. Strigari, *New J. Phys.* **11**, 105011 (2009), [arXiv:0903.3630](#).
4. J. Billard, L. Strigari, and E. Figueroa-Feliciano, *Phys. Rev.* **D89**, 023524 (2014), [arXiv:1307.5458](#).
5. R. F. Lang *et al.*, *Phys. Rev.* **D94**, 103009 (2016), [arXiv:1606.09243](#).
6. L. Baudis *et al.*, *JCAP* **01**, 044 (2014), [arXiv:1309.7024](#).
7. J. L. Newstead, L. E. Strigari, and R. F. Lang, *Phys. Rev.* **D99**, 043006 (2019), [arXiv:1807.07169](#).
8. B. Dutta *et al.*, *Phys. Lett.* **B773**, 242-246 (2017), [arXiv:1705.00661](#).
9. D. Aristizabal Sierra, N. Rojas, and M. H. G. Tytgat, *JHEP* **03**, 197 (2018), [arXiv:1712.09667](#).
10. M. C. Gonzalez-Garcia *et al.*, *JHEP* **07**, 019 (2018), [arXiv:1803.03650](#).
11. J. Billard, L. E. Strigari, and E. Figueroa-Feliciano, *Phys. Rev.* **D91**, 095023 (2015), [arXiv:1409.0050](#).
12. D. Akimov *et al.* (COHERENT Collaboration), *Science* **357**, no. 6356, 1123 (2017), [arXiv:1708.01294](#).
13. G. Bellini *et al.* (Borexino Collaboration), *Nature* **512**, 383 (2014).
14. G. Bellini *et al.* (Borexino Collaboration), *Phys. Rev. Lett.* **107**, 141302 (2011), [arXiv:1104.1816](#).
15. G. Bellini *et al.* (Borexino Collaboration), *Phys. Rev. Lett.* **108**, 051302 (2012), [arXiv:1110.3230](#).
16. M. Agostini *et al.* (Borexino Collaboration), *Phys. Rev.* **D100**, 082004 (2019), [arXiv:1707.09279](#).
17. M. Agostini *et al.* (Borexino Collaboration), *Nature* **562**, 505 (2018).
18. G. Bellini *et al.* (Borexino Collaboration), *Phys. Rev.* **D82**, 033006 (2010), [arXiv:0808.2868](#).
19. M. Agostini *et al.* (Borexino Collaboration), *Phys. Rev.* **D101**, 062001 (2020), [arXiv:1709.00756](#).
20. K. Abe *et al.* (Super-Kamiokande Collaboration), *Phys. Rev.* **D83**, 052010 (2011), [arXiv:1010.0118](#).
21. S. Abe *et al.* (KamLAND Collaboration), *Phys. Rev. C* **84**, 035804 (2011), [arXiv:1106.0861](#).
22. B. Aharmim *et al.* (SNO Collaboration), *Phys. Rev.* **C88**, 025501 (2013), [arXiv:1109.0763](#).
23. M. Anderson *et al.* (SNO+ Collaboration), *Phys. Rev. D* **99**, 012012 (2018), [arXiv:1812.03355](#).
24. D. Akimov *et al.* (COHERENT Collaboration), *Science* **357**, 1123-1126 (2017), [arXiv:1708.01294](#).
25. A. Serenelli, *Eur. Phys. J. A* **52** (2016) 4, 78, [arXiv:1601.07179](#).
26. M. Asplund *et al.*, *Ann. Rev. Astron. and Astrophys.* **47**, 481 (2009), [arXiv:0909.0948](#).
27. N. Grevesse and A. J. Sauval, *Space Sci. Rev.* **85**, 161 (1998).
28. A. Serenelli *et al.*, *Astrophys. J.* **705**, L123 (2009), [arXiv:0909.2668](#).
29. J. Bergstrom *et al.*, *JHEP* **03**, 132 (2016), [arXiv:1601.00972](#).
30. M. Agostini *et al.* (Borexino Collaboration), [arXiv:2005.12829](#).
31. K. S. Kumar *et al.*, *Ann. Rev. Nucl. Part. Sci.* **63**, 237 (2013), [arXiv:1302.6263](#).
32. M. Maltoni and A. Y. Smirnov, *Eur. Phys. J. A* **52**, 87 (2016), [arXiv:1507.05287](#).
33. H. Davoudiasl, H.-S. Lee, and W. J. Marciano *Phys. Rev.* **D92**, 055005 (2015), [arXiv:1507.00352](#).
34. Brookhaven National Laboratory, [national nuclear data center](#) (2015).
35. E. Aprile *et al.* (XENON Collaboration), *Eur. Phys. J.* **C77**, 890 (2017), [arXiv:1705.01828](#).
36. E. Aprile *et al.* (XENON Collaboration), *Eur. Phys. J.* **C77**, 358 (2017), [arXiv:1702.06942](#).
37. M. Murra, Intrinsic background reduction by cryogenic distillation for the XENON1T darkmatter experiment, PhD thesis, 2019.
38. E. Aprile *et al.* (XENON Collaboration), *Phys. Rev.* **D99**, 112009 (2019), [arXiv:1902.11297](#).

-
39. F. Agostini *et al.* (DARWIN Collaboration), [arXiv:2003.13407](#).
 40. C. Wittweg *et al.*, 2020, [arXiv:2002.04239](#).
 41. M. Doi and T. Kotanit, *Progress of Theoretical Physics* **87**, 5 (1992).
 42. E. Aprile *et al.* (XENON Collaboration), *Nature* **568**, 7753 (2019), [arXiv:1904.11002](#).
 43. N. Vinyoles *et al.*, *Astrophys. J.* **835**, 202 (2017), [arXiv:1611.09867](#).
 44. F. Capozzi *et al.*, *Phys. Rev.* **D95**, 096014 (2017), [arXiv:1703.04471](#).
 45. W. J. Marciano and Z. Parsa, *J. Phys.* **G29**, 2629 (2003), [arXiv:hep-ph/0403168](#).
 46. J. A. Formaggio and G. P. Zeller, *Rev. Mod. Phys.* **84**, 1307 (2012), [arXiv:1305.7513](#).
 47. J. Erler and M. J. Ramsey-Musolf, *Phys. Rev.* **D72**, 073003 (2005), [arXiv:hep-ph/0409169](#).
 48. E. Aprile *et al.* (XENON Collaboration), [arXiv:2003.03825](#).
 49. A. Sh. Georgadze *et al.*, *Astropart. Phys.* **7**, 173 (1997).
 50. P. C. Mahalanobis, *Proceedings of the National Institute of Sciences of India* **2**, 49 (1936).